Received 19 June 2024; revised 13 July 2024; accepted 15 July 2024. Date of publication 24 July 2024; date of current version 29 July 2024.

Digital Object Identifier 10.1109/OJCOMS.2024.3430051

Outage Performance of RIS-Assisted AmBC-NOMA Cooperative V2I Communications

AHMED SAMIR^{® 1,2} (Member, IEEE), AHMED S. IBRAHIM^{® 3} (Senior Member, IEEE), MAHMOUD H. ISMAIL^{® 1,4} (Senior Member, IEEE), BASEM M. ELHALAWANY^{® 2,5} (Senior Member, IEEE), AND MOHAMED ELSAYED^{® 1,2} (Member, IEEE)

¹Department of Electrical Engineering, American University of Sharjah, Sharjah, UAE

² Faculty of Engineering at Shoubra, Benha University, Benha 13511, Egypt

³Electrical and Computer Engineering Department, Florida International University, Miami, FL 33174, USA

CORRESPONDING AUTHOR: M. H. ISMAIL (e-mail: mhibrahim@aus.edu).

The work of Ahmed Samir, Mahmoud H. Ismail, and Mohamed Elsayed was supported by the American University of Sharjah through the Faculty Research Grants (FRG) Program under Award FRG22-C-E13 and Award FRG23-C-E12. The work of Ahmed S. Ibrahim was supported in part by the National Science Foundation under Award CNS-2144297.

ABSTRACT Vehicle-to-infrastructure (V2I) communication facilitates seamless interaction between vehicles and the surrounding infrastructure. Recently, there has been a notable surge in research interest in ambient backscatter communications (AmBC), primarily due to its ability to enable battery-free communication. Concurrently, reconfigurable intelligent surfaces (RISs) have garnered attention as a promising technology, particularly for the advancement of cellular systems beyond 5G. Additionally, non-orthogonal multiple access (NOMA) assumes a pivotal role in enhancing spectrum utilization. This paper proposes a new RIS-enhanced NOMA-AmBC system where all channels are characterized by Nakagami-m fading and with the main objective of assessing the performance of such system. To this end, new closed-form expressions for the outage probabilities (OPs) were derived under the practical assumption of imperfect successive interference cancellation (SIC). In addition, to gain a deep insight into the system's performance, we derived asymptotic, upper-bound, and lower-bound expressions for the OPs. Furthermore, we proposed a power allocation optimization problem to achieve an outage-optimal performance. To validate the analytical results, we conducted extensive investigations using Monte Carlo simulations, which indicates a high degree of consistency. Moreover, our results underscore the remarkable performance improvements achieved by the RIS-assisted AmBC-NOMA system when compared to both the traditional benchmark AmBC-NOMA system and the RIS-assisted orthogonal multiple access (AmBC-OMA) counterparts.

INDEX TERMS Ambient backscatter communications, non-orthogonal multiple access, reconfigurable intelligent surfaces, vehicle-to-infrastructure, outage probability, imperfect SIC, Nakagami-*m*.

I. INTRODUCTION

VOLUME 5, 2024

THE advancement of intelligent transportation systems (ITS) is expected to enhance traffic efficiency, control, reliability, and passenger safety [1], [2]. Vehicle-to-infrastructure (V2I) communication is identified as a promising technology for achieving these improvements [3].

However, challenges persist in current transportation systems that necessitate further investigation in spite of the recent deployment of 5G and the anticipated introduction of beyond 5G (B5G) systems. V2I communication systems are highly sensitive to reliability, making the outage probability framework essential in practical V2I communication

4371

⁴Department of Electronics and Communications Engineering, Faculty of Engineering, Cairo University, Giza 12613, Egypt

⁵Electronics and Communication Engineering Department, Kuwait College of Science and Technology, Doha 93004, Kuwait

for autonomous driving and ITS [4]. Another concern revolves around the high data rate and massive connectivity demands in V2I networks, which may exceed the capabilities of existing orthogonal multiple access (OMA) resources. Consequently, novel spectrum access technologies are imperative to ensure high spectral efficiency within B5G V2I networks. In recent times, non-orthogonal multiple access (NOMA), employing power domain multiplexing, has emerged as a prominent air interface technology known for its superior spectral efficiency and minimal latency [5], [6]. A key attribute of NOMA is its ability to concurrently accommodate multiple devices on the same spectrum resource [7], [8], [9], which is realized through two distinct techniques: superposition coding (SC) and successive interference cancellation (SIC).

Another key concern in V2I systems is the substantial growth of the number of roadside units (RSU) involved, which, when coupled with their diverse quality of service (QoS) requirements, poses a significant energy consumption challenge [10]. In response to this, both academia and industry are actively exploring various energy-efficient solutions to address this critical situation. Some potential strategies involve leveraging existing ambient radio frequency (RF) signals for communication within the V2I system, which is commonly known as ambient backscatter communications (AmBC). The core idea behind AmBC involves the development of a device capable of harvesting energy from existing RF signals, thus enabling it to power its circuit while simultaneously modulating and reflecting its own information [11]. These unique attributes position the AmBC system as a strong candidate technology for battery-free communication in the B5G era. Over the past few years, researchers have extensively investigated the performance of these devices in various communication scenarios in combination with the NOMA technology. For example, in [12], the authors proposed a symbiotic AmBC battery-free IoT system, that exploits a downlink transmission of a NOMA multiplexingenabled cellular network to permit an IoT spectrum-efficient uplink communication. Also, the authors in [13] introduced an AmBC-NOMA network specifically designed for ITS. In this network, a vehicle strategically chooses the optimal antenna to transmit a random power signal satisfying a uniform distribution to communicate with a covert vehicle. A cognitive AmBC-NOMA Internet-of-Vehicle (IoV) maritime transportation systems network was proposed in [14]. The authors explored the reliable and secure performance of the proposed system with in-phase and quadraturephase imbalance (IQI) at radio-frequency (RF) front-ends with the existence of an eavesdropper. In particular, they obtained analytical expressions for the outage probability (OP) and intercept probability. In addition, the authors in [15] provided an analytical framework for studying the impact of delayed QoS on the AmBC-NOMA systems, they provided an effective capacity analysis for a typical downlink scenario and proved that larger reflection coefficients at the backscatter device (BD) leads to increased effective

capacity for the BD but decreased effective capacities for the NOMA-users.

Notwithstanding the considerable potential of AmBC, this communication paradigm faces two major challenges: weak backscatter signals and the presence of strong direct interference signals. These challenges contribute to a notable degradation in the performance of AmBC [16]. On another related front, an emerging and promising technology that is expected to be deployed in B5G systems is reconfigurable intelligent surfaces (RIS), which has recently garnered considerable attention. RIS involves the deployment of passive reflecting elements to dynamically reconfigure the wireless channel environment [4], [17]. Recently, there has been a growing focus on RIS-assisted vehicular communications [4], [18]. In [4], for instance, a model of RIS-assisted V2I network model in the highway environment was proposed. Assuming Rayleigh fading channels, the authors derived the downlink OP of the proposed V2I system while considering inter-cell interference. The secrecy OP in the presence of an eavesdropper was analyzed in [18] for both Rayleigh-fading-based vehicle-to-vehicle (V2V) and V2I communication when the RIS acts as a relay aid

Based on the above literature, the combination of RIS and AmBC systems presents a potential direction for substantial performance improvement. For example, in [19], using the moment-generating function approach, the authors derived an expression for the symbol error probability and provided tight upper bounds for both fully correlated and mutually independent channels for a large intelligent surface-aided backscatter communication systems.

The investigation of RIS-assisted downlink NOMA was introduced in [20], [21], [22], where the authors in [20] derived the OP closed-form expressions concerning both near and far users, and based on the analysis, they reached the fact that adding a RIS helps NOMA systems to improve the performance when compared to a RIS-OMA one. While in [21], the authors investigated the enhancement of V2V communication systems utilizing RIS and simultaneous transmitting and reflecting intelligent omni-surfaces (STAR-IOS). By integrating these technologies, the paper addressed the performance under both NOMA and OMA schemes in environments characterized by composite fading channels modeled with the Fisher-Snedecor \mathcal{F} -distribution. The authors demonstrated significant performance improvements in terms of outage probability, ergodic capacity, and energy efficiency when using RIS/STAR-IOS configurations, particularly under NOMA schemes compared to OMA.

Recently, by incorporating RIS into AmBC-NOMA systems, notable enhancements can be realized, particularly in terms of amplifying backscatter signals and effectively suppressing interference. The authors in [23] proposed an innovative system that enhances backscatter communication links using RIS in conjunction with NOMA technology. This paper addressed the double fading effect inherent in

TABLE 1. Comparison of this paper with other related work.

Ref.	AmBC	NOMA	RIS	Imperfect	Outage	Asymptotic	Bounds on	Optimization	Diversity	Channel
Kei.	system	NOMA	KIS	SIC	probability	analysis	outage	Optimization	order	fading
[13]	✓	✓			✓	✓		✓		Quasi-Rayleigh
[14]	✓	✓			✓	✓				Rayleigh
[18]		✓	✓	✓	✓	✓			✓	Rayleigh
[20]	✓		✓							Gaussian
[21]		✓	✓	✓	✓	✓				Rayleigh
[22]		✓	✓		✓					Fisher-Snedecor
[24]	✓	✓	✓					✓		Rician
[25]	✓		✓					✓		Rayleigh
[26]		✓	✓					√		Rician & Rayleigh
This paper	✓	✓	✓	√	√	✓	✓	✓	✓	Nakagami- m

NOMA-assisted backscatter communication (RIS-AmBC-NOMA) systems by introducing a joint optimization problem for power reflection coefficients at the backscatter devices and phase shifts at the RIS. Employing a combination of alternating optimization, successive convex approximation, and manifold optimization algorithms, the study demonstrated significant improvements in the data rate of the proposed RIS-AmBC-NOMA system over conventional AmBC-NOMA systems without RIS. This paper addressed the collaboration between RIS, AmBC, and NOMA from an optimization perspective. However, there remains a research gap in the performance analysis of this collaboration.

A. MOTIVATION

Based on the literature, we can conclude that the fundamental challenges that face V2I communication systems are the RSU energy consumption challenge, the weakness of the RSU signal, and the spectrum utilization efficiency. To overcome the RSU energy consumption challenge, we replace the battery-operated RSU with a backscatter device that relies on ambient power in its operation. To handle the remaining challenges, we deploy a RIS and exploit a NOMA multiplexing scheme in the proposed system. Despite extensive work on AmBC, NOMA, and RIS networks, as summarized in Table 1, much of the focus has been on addressing singular or dual aspects of these challenges. To the best of our knowledge, none have addressed all of these three challenges altogether. Motivated by this, we propose a system model aimed to gain the benefits of the RIS technology when combined with NOMA and AmBC technologies within the context of V2I communication. The proposed RIS-enhanced AmBC-NOMA cooperative V2I communication model specifically integrates RIS-AmBC to facilitate information transmission from backscatter nodes to their vehicular destinations, leveraging NOMA to augment spectrum efficiency. In particular, we investigate the performance of the proposed system in terms of outage probability and to gain more insight, we derive an asymptotic outage probability and formulate and solve a power allocation optimization problem. Accordingly, the proposed system has various practical applications within autonomous

vehicles and ITS. For example, it facilitates reliable and lowlatency communication for autonomous vehicles, ensuring safe and efficient operations by enabling real-time interaction with traffic lights, road signs, and other infrastructure components. In the context of smart cities, the framework supports the deployment of wireless sensor networks and IoT devices, with energy-efficient communication provided by AmBC ensuring sustainability and scalability.

B. CONTRIBUTIONS

In consideration of the aforementioned motivation and challenges, and to the best of our knowledge, this paper presents the first analysis of the outage probability performance for the proposed RIS-enhanced AmBC-NOMA cooperative V2I communication model in the open literature. The main contributions of this paper are summarized as follows:

- Characterizing the statistical distribution of the received signal-to-interference-plus-noise ratio (SINR) of the proposed system at the end users, by deriving the probability density function (PDF) via the Central Limit Theorem (CLT) and moment-based Gamma approximation, assuming that the wireless channels are characterized by Nakagami-*m* fading with additive white Gaussian noise (AWGN) under the practical assumption of imperfect SIC at receivers.
- Deriving new closed-form expressions for the outage probabilities (OPs) at each end user and the total system outage.
- Deriving asymptotic expressions and diversity order for the OPs assuming high base station transmission power, also we derived upper and lower bounds on the OPs to be used for optimizing the NOMA power allocations.
- Formulating and solving a power allocation optimization problem to obtain NOMA optimal power allocation factors to minimize the system OP.
- Validating the analytical derivations through extensive Monte-Carlo simulations and studying the impact of system parameters on the OPs performance.
- Comparing the proposed system and both the traditional benchmark AmBC-NOMA system (with no RIS) and the RIS-assisted AmBC-OMA system.

VOLUME 5, 2024 4373

TABLE 2. Description of important parameters.

Parameter	Description				
P	Base station transmit power.				
β_i	Power reflection coefficient of the i^{th} BD.				
r_k	Reflection coefficient of the k^{th} RIS element.				
s_i	s_i Message signal of the i^{th} BD.				
Z_i	Backscattered signal at the i^{th} BD.				
y_{D_j}	Received signal at j^{th} vehicles.				
$\gamma_{D_j}^i$ Received SINR at D_j to detect its message s_i .					
ε	ε Residual power factor due to imperfect SIC.				
T_i	T_i Channel gain between CS and i^{th} BD.				
$L_{k,i}$	$L_{k,i}$ Channel gain between i^{th} BD and k^{th} RIS element				
$g_{k,j}$	$g_{k,j}$ Channel gain between k^{th} RIS element and D_j .				
h_{ij}	h_{ij} Channel gain between i^{th} BD and D_j .				
w_{j}	w_j Additive white Gaussian noise at D_j .				
k_x , θ_x	k_x, θ_x Gamma distribution parameters of channel x				
m_x	m_x Nakagami- m severity factor of channel x				
γ^i_{th}	SINR threshold for receiving s_i .				
OP_{D_j}	Outage probability at D_j .				
OP_{sys}	Overall system outage probability.				

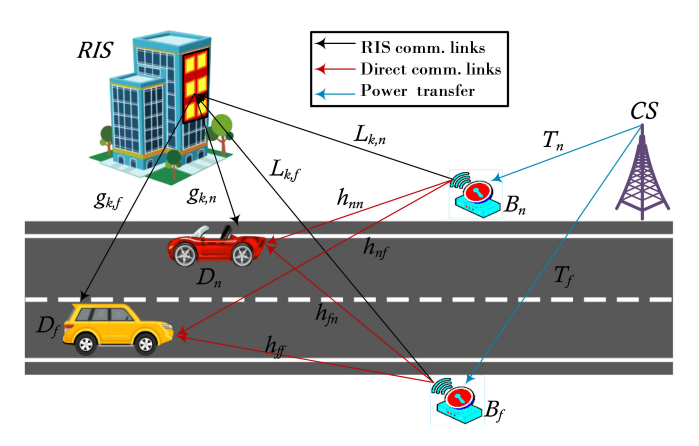


FIGURE 1. RIS-enhanced AmBC-NOMA cooperative V2I System model.

The rest of the paper is organized as follows. The system model is introduced in Section II. The performance of the considered system is analytically evaluated by deriving the OPs in Section III. The power allocation optimization problem is then proposed and solved in Section IV. Analytical and simulation results are discussed and compared with benchmark systems in Section V before the conclusions are finally provided in Section VI. A description of important parameters is provided in Table 2.

II. SYSTEM MODEL

We consider a RIS-enhanced AmBC-NOMA cooperative V2I communication system, as illustrated in Fig. 1. The system consists of an ambient carrier source (CS), two BDs denoted as (B_n, B_f) , which act as RSU, a RIS with K reflecting elements, and two vehicles, (D_n, D_f) , which act as the backscatter receivers (BRs). In this paper, we

consider a low-speed vehicular mobility model¹ where the vehicles remain static during consecutive time slots of the transmission, also we make the following assumptions: 1) The CS, BDs, and BRs use a single antenna; 2) The BRs perform imperfect SIC; 3) The channels between different devices are independent and characterized by Nakagami-*m* fading; 4) The channel state information (CSI) is considered to be perfect.²

In the presented scenario, the CS transmits a sinusoidal carrier signal, which represents the ambient power source that supports the BDs in their operation and in transmitting their information. Specifically, the CS transmits a sinusoidal carrier signal, while the BDs modulate their information over this incident carrier signal and backscatter it to the BRs. For the sake of enhancing spectrum efficiency, we assume that each BD modulates a message intended for a specific BR at different power allocation levels via NOMA technology. We assume that B_n and B_f want to communicate with their associated vehicles, D_n and D_f , respectively, and that D_n is a NOMA-near user while D_f is a NOMA-far one. The backscattered signal at the i^{th} BD can be written as

$$Z_i = \sqrt{P\beta_i} T_i s_i, \tag{1}$$

where $i \in \{n, f\}$, P is the total power transmitted from CS, s_i represents the message signal of the i^{th} BD with a unit mean power, β_i denotes the power reflection coefficient of the i^{th} BD, which plays the role of the NOMA power allocation in determining the decoding order. Without loss of generality, we assume that $\beta_n < \beta_f$, $\beta_n + \beta_f = 1$. T_i denotes the gain of the wireless channel between CS and BDs, which is assumed to be Nakagami-m faded, i.e., $T_i \sim$ Nakagami-m (m_{T_i} , 1). The backscattered signal will reach the intended BRs through two different paths, i.e., the direct link and the RIS-supported link, so the received signal at the far and near vehicles can be expressed as

$$y_{D_j} = \sum_{i \in \{f,n\}} \left(h_{ij} + \sum_{k=1}^K L_{k,i} r_k g_{k,j} \right) Z_i + \omega_j,$$
 (2)

where $j \in \{n, f\}$, h_{ij} represents the gain of the direct link between i^{th} BD and j^{th} BR, while $L_{k,i}$ denotes the channel gain from the i^{th} BD to the k^{th} RIS element and $g_{k,j}$ denotes the reflected channel gain from the k^{th} RIS element toward the j^{th} BR. All these channels are assumed to follow Nakagami-m fading with severity factors of m_{λ} and a

¹This is a realistic assumption, especially at road intersections and urban scenarios where the vehicles tend to drive slowly across the junctions and intersections.

²Channel estimation in AmBC systems is radically different from that for conventional wireless systems due to the power and processing limitations that prevent tags from transmitting training symbols. In [26], the authors proposed a blind channel estimator that focuses on the RIS-assisted backscatter communication system. The estimator is based on the expectation-maximization algorithm to acquire the modulus values of channel parameters. Also, in [27], the authors provide a good summary in Table I that delineates the latest research endeavors in the field of CSI of AmBC systems. Such estimation techniques can be employed in the considered system.

unity expectation where $\lambda \in \{h_{ij}, L_{k,i}, g_{k,j}\}$. Furthermore, ω_j represents AWGN with $\omega_j \sim \mathcal{CN}(0, \sigma_{\omega_j}^2)$ and $r_k = |r_k|e^{j\varphi_k}$ is the reflection coefficient of the k^{th} RIS element. To maximize the received signal strength, we assume that all magnitudes $|r_k| = 1$, while φ_k is the k^{th} RIS element adjustable phase. We assumed an ideal phase shift for each element, i.e., $\varphi_k = \angle h_{ij} - (\angle L_{k,i} + \angle g_{k,j})$, so that the received signals at each vehicle from all channels are in-phase [28], [29], [30]. Accordingly, we can write

$$y_{D_j} = \sum_{i \in \{f, n\}} \left(\left| h_{ij} \right| + \underbrace{\sum_{k=1}^K \left| L_{k,i} \right| \left| g_{k,j} \right|}_{\alpha_{ij}} \right) Z_i \angle h_{ij} + \omega_j. \quad (3)$$

Therefore, the received SINR at D_f to detect its own message s_f is

$$\gamma_{D_f}^f = \frac{\rho \beta_f \xi_f^2 |T_f|^2}{\rho \beta_n \xi_{nf}^2 |T_n|^2 + 1}.$$
 (4)

Following the NOMA principle, D_n decodes s_f firstly and then applies the SIC operation, which is assumed to be imperfect, to decode its own message s_n . So, the SINRs for decoding s_f and s_n at D_n are expressed as [31], [32]

$$\gamma_{D_n}^f = \frac{\rho \beta_f \xi_{fn}^2 |T_f|^2}{\rho \beta_n \xi_{-1}^2 |T_n|^2 + 1},\tag{5}$$

$$\gamma_{D_n}^n = \frac{\rho \beta_n \xi_{nn}^2 |T_n|^2}{\epsilon \rho \beta_f \xi_{fn}^2 |T_f|^2 + 1},\tag{6}$$

respectively, where in (4)–(6), the transmitted SNR $\rho = P/\sigma_{w_f}^2 = P/\sigma_{w_n}^2$, and $0 < \varepsilon < 1$ is the residual power factor due to imperfect SIC [9].

In the following, we highlight the distributions of the three SINRs obtained above. Based on the CLT and the moment-based Gamma approximation approach, assuming a large number of RIS elements, α_{ij} can be approximated as a Gamma distribution [33], [34], such that $\alpha_{ij} \sim \Gamma(k_{\alpha_{ij}}, \theta_{\alpha_{ij}})$ where

$$k_{\alpha_{ij}} = \frac{\left(E_{\alpha_{ij}}^{(1)}\right)^2}{E_{\alpha_{ij}}^{(2)} - \left(E_{\alpha_{ij}}^{(1)}\right)^2}, \quad \theta_{\alpha_{ij}} = \frac{E_{\alpha_{ij}}^{(2)} - \left(E_{\alpha_{ij}}^{(1)}\right)^2}{E_{\alpha_{ij}}^{(1)}}, \quad (7)$$

with $\mathbf{E}_{X}^{(p)}$ being the p^{th} moment of X such that

$$E_{\alpha_{ij}}^{(p)} = K \frac{\Gamma(m_{L_{k,i}} + p/2) \Gamma(m_{g_{k,j}} + p/2)}{(m_{L_{k,i}} m_{g_{k,j}})^{p/2} \Gamma(m_{L_{k,i}}) \Gamma(m_{g_{k,j}})},$$
(8)

where $\Gamma(\cdot)$ is the well-known gamma function. Consequently, according to [33], [34], ξ_{ij} can be

approximated by a Gamma distribution such that $\xi_{ij} \sim \Gamma(k_{\xi_{ii}}, \theta_{\xi_{ii}})$ where

$$k_{\xi_{ij}} = \frac{\left(E_{\xi_{ij}}^{(1)}\right)^{2}}{E_{\xi_{ij}}^{(2)} - \left(E_{\xi_{ij}}^{(1)}\right)^{2}}, \quad \theta_{\xi_{ij}} = \frac{E_{\xi_{ij}}^{(2)} - \left(E_{\xi_{ij}}^{(1)}\right)^{2}}{E_{\xi_{ij}}^{(1)}}, \quad (9)$$

and

$$\mathbf{E}_{\xi_{ii}^{2}}^{(1)} = \mathbf{E}_{h_{ij}}^{(2)} + \mathbf{E}_{\alpha_{ij}}^{(2)} + 2\mathbf{E}_{h_{ij}}^{(1)}\mathbf{E}_{\alpha_{ij}}^{(1)},\tag{10}$$

$$E_{\xi_{ij}^{2}}^{(2)} = E_{h_{ij}}^{(4)} + E_{\alpha_{ij}}^{(4)} + 6E_{h_{ij}}^{(2)}E_{\alpha_{ij}}^{(1)} + 4E_{h_{ij}}^{(3)}E_{\alpha_{ij}}^{(1)} + 4E_{h_{ij}}^{(1)}E_{\alpha_{ij}}^{(3)},$$
(11)

$$E_{h_{ij}}^{(p)} = \frac{\Gamma(m_{h_{ij}} + p/2)}{m_{h_{ii}}^{p/2} \Gamma(m_{h_{ij}})}.$$
 (12)

Since T_i is characterized by a Nakagami-m distribution, i.e., $|T_i|^2 \sim \Gamma(m_{T_i}, \frac{1}{m_{T_i}})$, and T_i^2 , ξ_{ij}^2 are independent and non-identically distributed (i.n.i.d.), consequently $\delta_{ij} = \xi_{ij}^2 |T_i|^2$ follows a gamma distribution, viz., $\delta_{ij} \sim \Gamma(k_{\delta_{ij}}, \theta_{\delta_{ij}})$ where

$$k_{\delta ij} = \frac{\left(E_{\delta ij}^{(1)}\right)^2}{E_{\delta ij}^{(2)} - \left(E_{\delta ij}^{(1)}\right)^2}, \quad \theta_{\delta ij} = \frac{E_{\delta ij}^{(2)} - \left(E_{\delta ij}^{(1)}\right)^2}{E_{\delta ij}^{(1)}}, \quad (13)$$

and
$$\mathbf{E}_{\delta_{ij}}^{(p)} = \mathbf{E}_{|T_i|^2}^{(p)} \mathbf{E}_{\xi_{ij}^2}^{(p)}, \mathbf{E}_{|T_i|^2}^{(1)} = 1, \mathbf{E}_{|T_i|^2}^{(2)} = \frac{\Gamma(m_{T_i} + 2)}{m_{T_i}^2 \Gamma(m_{T_i})}.$$
 Finally, to derive the PDFs of different SINRs in (4)–(6),

Finally, to derive the PDFs of different SINRs in (4)–(6), we can rewrite them as $\gamma_{D_f}^f = \frac{\psi_{ff}}{\chi_{nf}}$, $\gamma_{D_n}^f = \frac{\psi_{fn}}{\chi_{nn}}$, and $\gamma_{D_n}^n = \frac{\psi_{nn}}{\chi_{fn}}$, where $\psi_{ij} \sim \Gamma(k_{\delta_{ij}}, \rho \beta_i \theta_{\delta_{ij}})$ based on the gamma distribution scaling property. According to [35] and using the shifted gamma distribution, χ_{ij} is also gamma distributed as $\chi_{ij} \sim \Gamma(k_{\chi_{ii}}, \theta_{\chi_{ij}})$, where

$$k_{\chi_{ij}} = \frac{\left(E_{\chi_{ij}}^{(1)}\right)^2}{E_{\chi_{ij}}^{(2)} - \left(E_{\chi_{ij}}^{(1)}\right)^2}, \quad \theta_{\chi_{ij}} = \frac{E_{\chi_{ij}}^{(2)} - \left(E_{\chi_{ij}}^{(1)}\right)^2}{E_{\chi_{ij}}^{(1)}}, \quad (14)$$

and

$$\mathbf{E}_{\chi_{ij}}^{(1)} = \begin{cases} \rho \beta_n \mathbf{E}_{\delta_{ij}}^{(1)} + 1 & ij \in \{nn, nf\} \\ \epsilon \rho \beta_f \mathbf{E}_{\delta_{ij}}^{(1)} + 1 & ij \in \{fn\} \end{cases}, \tag{15}$$

$$\mathbf{E}_{\chi ij}^{(2)} = \begin{cases} \rho^2 \beta_n^2 \mathbf{E}_{\delta ij}^{(2)} + 2\rho \beta_n \mathbf{E}_{\delta ij}^{(1)} + 1 & ij \in \{nn, nf\} \\ \varepsilon^2 \rho^2 \beta_f^2 \mathbf{E}_{\delta ij}^{(2)} + 2\varepsilon \rho \beta_f \mathbf{E}_{\delta ij}^{(1)} + 1 & ij \in \{fn\} \end{cases} . \tag{16}$$

Finally, in accordance with the premise that if $\psi \sim \Gamma(k_{\delta}, \rho\beta\theta_{\delta})$ and $\chi \sim \Gamma(k_{\chi}, \theta_{\chi})$ represent two independent Gamma-distributed random variables, the ratio $\gamma = \psi/\chi$ follows a Beta prime distribution [36], $\gamma \sim \beta'(k_{\delta}, k_{\chi}, 1, \frac{\rho\beta\theta_{\delta}}{\theta_{\chi}})$ and has a PDF of

$$f_{\gamma}(x) = \frac{\theta_{\chi} \left(\frac{\theta_{\chi} x}{\rho \beta \theta_{\delta}}\right)^{k_{\delta} - 1}}{\rho \beta \theta_{\delta} \left(1 + \frac{\theta_{\chi} x}{\rho \beta \theta_{\delta}}\right)^{k_{\delta} + k_{\chi}} \mathbf{B}(k_{\delta}, k_{\chi})},\tag{17}$$

where γ donates each of the three different SINRs in (4)–(6).

VOLUME 5, 2024 4375

III. OUTAGE PROBABILITY ANALYSIS

Outage can result in the incomplete delivery of traffic information, impacting road safety. Consequently, OP is regarded as a critical quality of service metric [37]. In this section, an extensive performance analysis of the proposed system is conducted, focusing on the OP. The OP is defined as the probability of the receiver being unable to decode the message, an event that transpires when the received SINR drops below a specified threshold value. We derive the analytical closed-form, asymptotic, and bounds on OPs.

A. OUTAGE PROBABILITY AT DF

The outage event at D_f occurs if it can not decode s_f , i.e., when the received SINR at D_f falls bellow a specific threshold, which can be formulated as

$$OP_{D_f} = P\left(f_{\gamma_{D_f}^f}(x) < \gamma_{th}^f\right) = \int_{0}^{\gamma_{th}^f} f_{\gamma_{D_f}^f}(x) dx,$$
 (18)

where $\gamma_{th}^f = 2^{R_f} - 1$ and R_f is the target data rate for receiving s_f . Substituting (4) and (17) into (18), we get

$$OP_{D_f} = \frac{\theta_{\chi_{nf}}}{\rho \beta_f \theta_{\delta_{ff}} B(k_{\delta_{ff}}, k_{\chi_{nf}})} \int_0^{\gamma_{th}^f} \frac{\left(\frac{\theta_{\chi_{nf}} x}{\rho \beta_f \theta_{\delta_{ff}}}\right)^{k_{\delta_{ff}} - 1}}{\left(1 + \frac{\theta_{\chi_{nf}} x}{\rho \beta_f \theta_{\delta_{ff}}}\right)^{k_{\delta_{ff}} + k_{\chi_{nf}}}} dx.$$
(19)

By applying the variable transformation $z = \theta_{\chi_{nf}} x / \rho \beta_f \theta_{\delta_{ff}}$, we can write

$$OP_{D_f} = \frac{1}{B(k_{\delta_{ff}}, k_{\chi_{nf}})} \int_{0}^{\eta_{ff}} \frac{(z)^{k_{\delta_{ff}} - 1}}{(1 + z)^{k_{\delta_{ff}} + k_{\chi_{nf}}}} dz, \qquad (20)$$

where $\eta_{ff} = \theta_{\chi_{nf}} \gamma_{th}^f / \rho \beta_f \theta_{\delta_{ff}}$, using [38, Eq. (3.194.1)], we obtain a closed-form expression of OP_{D_f} as

$$OP_{D_f} = \frac{\eta_{ff}^{k_{\delta_{ff}}} {}_{2}F_{1}(k_{\delta_{ff}} + k_{\chi_{nf}}, k_{\delta_{ff}}; 1 + k_{\delta_{ff}}; -\eta_{ff})}{k_{\delta_{ff}}B(k_{\delta_{ff}}, k_{\chi_{nf}})}, \quad (21)$$

where ${}_2F_1(.,.;.;.)$ is the Gauss hypergeometric function [38, eq. (9.14.1)].

B. OUTAGE PROBABILITY AT DN

The outage event at D_n occurs when it can not decode s_f or s_n ; this is due to the NOMA SIC concept that involves

receiving s_f and canceling it before receiving s_n . This can be formulated as

$$OP_{D_n} = 1 - P\left(f_{\gamma_{D_n}^f}(x) > \gamma_{th}^f, f_{\gamma_{D_n}^n}(x) > \gamma_{th}^n\right)$$

$$\stackrel{(a)}{=} 1 - \left(1 - \underbrace{P(f_{\gamma_{D_n}^f}(x) < \gamma_{th}^f)}_{B_1}\right) \left(1 - \underbrace{P(f_{\gamma_{D_n}^n}(x) < \gamma_{th}^n)}_{B_2}\right),$$

$$(22)$$

where $\gamma_{th}^n = 2^{R_n} - 1$ with R_n being the target data rate for receiving s_n and (a) is a consequence of the independence between $f_{\gamma_{D_n}^f}$ and $f_{\gamma_{D_n}^n}$. Furthermore, we can write

$$B_{1} = \int_{0}^{\gamma_{th}^{f}} f_{\gamma_{D_{n}}^{f}}(x)dx, \qquad B_{2} = \int_{0}^{\gamma_{th}^{n}} f_{\gamma_{D_{n}}^{n}}(x)dx.$$
 (23)

Substituting (5), (6) and (17) into (23), we obtain

$$B_{1} = \frac{\theta_{\chi_{nn}}}{\rho \beta_{f} \theta_{\delta_{fn}} B(k_{\delta_{fn}}, k_{\chi_{nn}})} \int_{0}^{\gamma_{th}^{f}} \frac{\left(\frac{\theta_{\chi_{nn}} x}{\rho \beta_{f} \theta_{\delta_{fn}}}\right)^{k_{\delta_{fn}} - 1}}{\left(1 + \frac{\theta_{\chi_{nn}} x}{\rho \beta_{f} \theta_{\delta_{fn}}}\right)^{k_{\delta_{fn}} + k_{\chi_{nn}}}} dx,$$

$$B_{2} = \frac{\theta_{\chi_{fn}}}{\rho \beta_{f} \theta_{\delta_{nn}} B(k_{\delta_{nn}}, k_{\chi_{fn}})} \int_{0}^{\gamma_{th}^{n}} \frac{\left(\frac{\theta_{\chi_{fn}} x}{\rho \beta_{f} \theta_{\delta_{nn}}}\right)^{k_{\delta_{nn}} + k_{\chi_{fn}}}}{\left(1 + \frac{\theta_{\chi_{fn}} x}{\rho \beta_{f} \theta_{\delta_{nn}}}\right)^{k_{\delta_{nn}} + k_{\chi_{fn}}}} dx. (24)$$

Similar to OP_{D_f} , by applying the variable transformation and using [38, eq. (3.194.1)], we obtain a closed-form expression of OP_{D_n} as in (25) on bottom of the page, where $\eta_{fn} = \theta_{\chi_{nn}} \gamma_{th}^f / \rho \beta_f \theta_{\delta_{fn}}$, and $\eta_{nn} = \theta_{\chi_{fn}} \gamma_{th}^n / \rho \beta_n \theta_{\delta_{nn}}$.

C. TOTAL SYSTEM OUTAGE PROBABILITY

The total system outage OP_{sys} occurs if D_f fails to decode s_f or D_n fails to decode any of the two messages s_f , s_n . It is expressed as

$$OP_{sys} = 1 - P\left(f_{\gamma_{Df}^{f}}(x) > \gamma_{th}^{f}, f_{\gamma_{Dn}^{f}}(x) > \gamma_{th}^{f}, f_{\gamma_{Dn}^{n}}(x) > \gamma_{th}^{n}\right),$$

$$\stackrel{(b)}{=} 1 - \left(1 - P\left(f_{\gamma_{Df}^{f}}(x) < \gamma_{th}^{f}\right)\right)$$

$$\times \left(1 - P\left(f_{\gamma_{Dn}^{f}}(x) < \gamma_{th}^{f}\right)\right) \left(1 - P\left(f_{\gamma_{Dn}^{n}}(x) < \gamma_{th}^{n}\right)\right),$$

$$(26)$$

$$OP_{D_{n}} = 1 - \left(1 - \underbrace{\frac{\eta_{f_{n}}^{k_{\delta_{f_{n}}}} {}_{2}F_{1}(k_{\delta_{f_{n}}} + k_{\chi_{nn}}, k_{\delta_{f_{n}}}; 1 + k_{\delta_{f_{n}}}; -\eta_{f_{n}})}_{k_{\delta_{f_{n}}}B(k_{\delta_{f_{n}}}, k_{\chi_{nn}})}\right) \left(1 - \underbrace{\frac{\eta_{nn}^{k_{\delta_{nn}}} {}_{2}F_{1}(k_{\delta_{nn}} + k_{\chi_{f_{n}}}, k_{\delta_{nn}}; 1 + k_{\delta_{nn}}; -\eta_{nn})}_{k_{\delta_{nn}}B(k_{\delta_{nn}}, k_{\chi_{f_{n}}})}\right). \quad (25)$$

where (b) results from the independence between $f_{\gamma_{D_c}^f}$, $f_{\gamma_{D_c}^f}$ and $f_{\mathcal{V}_{D_n}^n}$. With the aid of definition of OP_{D_f} and $OP_{D_n}^{J}$, we can write OP_{sys} in terms of OP_{D_f} , B_1 , and B_2 as

$$OP_{sys} = 1 - (1 - OP_{D_f})(1 - B1)(1 - B2),$$
 (27)

substituting (21) and (24) into (27), we obtain a closed-form expression of OP_{sys} as in (28) on the bottom of the page.

D. ASYMPTOTIC OUTAGE PROBABILITY

A deep insight into the system performance under a high SNR regime is achieved by deriving asymptotic outage probabilities. At high SNR, i.e., $\rho \rightarrow \infty$, by substituting (15), (16) into (14) and performing some mathematical manipulations, we can rewrite $\theta_{\chi_{ii}}$ as

$$\theta_{\chi_{ij}}^{\infty} = \begin{cases} \rho \beta_n \theta_{\delta_{ij}} & ij \in \{nn, nf\} \\ \varepsilon \rho \beta_f \theta_{\delta_{ii}} & ij \in \{fn\} \end{cases}, \tag{29}$$

then we can write $\eta_{ff}^{\infty} = \beta_n \theta_{\delta_{nf}} \gamma_{th}^f / \beta_f \theta_{\delta_{ff}}, \quad \eta_{fn}^{\infty}$ $\beta_n \theta_{\delta_{nn}} \gamma_{th}^f / \beta_f \theta_{\delta_{fn}}$, and $\eta_{nn}^{\infty} = \varepsilon \beta_f \theta_{\delta_{fn}} \gamma_{th}^n / \beta_n \theta_{\delta_{nn}}$. Additionally, $k_{\chi_{ij}}$ can be simplified as

$$k_{\chi_{ij}}^{\infty} = \frac{\left(\rho\beta_{n}E_{\delta_{ij}}^{(1)}\right)^{2} + 2\rho\beta_{n}E_{\delta_{ij}}^{(1)} + 1}{\rho^{2}\beta_{n}^{2}E_{\delta_{ij}}^{(2)} + 2\rho\beta_{n}E_{\delta_{ij}}^{(1)} + 1 - \left(\rho\beta_{n}E_{\delta_{ij}}^{(1)}\right)^{2} - 2\rho\beta_{n}E_{\delta_{ij}}^{(1)} - 1}$$

$$= \frac{\left(\rho\beta_{n}E_{\delta_{ij}}^{(1)}\right)^{2} + 2\rho\beta_{n}E_{\delta_{ij}}^{(1)} + 1}{\rho^{2}\beta_{n}^{2}E_{\delta_{ij}}^{(2)} - \left(\rho\beta_{n}E_{\delta_{ij}}^{(2)}\right)^{2}} = \frac{\left(E_{\delta_{ij}}^{(1)}\right)^{2}}{E_{\delta_{ij}}^{(2)} - \left(E_{\delta_{ij}}^{(2)}\right)^{2}}, \quad (30)$$

thus, at $\rho \to \infty$, $k_{\chi_{ij}}^{\infty} = k_{\delta_{ij}}$. The asymptotic expressions of OP_{D_f} , B_1 , and B_2 can finally be given as

$$OP_{D_f}^{\infty} = \frac{\left(\eta_{ff}^{\infty}\right)^{k_{\delta_{ff}}} {}_{2}F_{1}\left(k_{\delta_{ff}} + k_{\delta_{nf}}, k_{\delta_{ff}}; 1 + k_{\delta_{ff}}; -\eta_{ff}^{\infty}\right)}{k_{\delta_{ff}} B\left(k_{\delta_{ff}}, k_{\delta_{nf}}\right)}, (31a)$$

$$B_{1}^{\infty} = \frac{\left(\eta_{fn}^{\infty}\right)^{k_{\delta_{fn}}} {}_{2}F_{1}\left(k_{\delta_{fn}} + k_{\delta_{nn}}, k_{\delta_{fn}}; 1 + k_{\delta_{fn}}; -\eta_{fn}^{\infty}\right)}{k_{\delta_{fn}} B\left(k_{\delta_{fn}}, k_{\delta_{nn}}\right)}, (31b)$$

$$B_{2}^{\infty} = \frac{\left(\eta_{nn}^{\infty}\right)^{k_{\delta_{nn}}} {}_{2}F_{1}\left(k_{\delta_{nn}} + k_{\delta_{fn}}, k_{\delta_{nn}}; 1 + k_{\delta_{nn}}; -\eta_{nn}^{\infty}\right)}{k_{\delta_{nn}} B\left(k_{\delta_{nn}}, k_{\delta_{fn}}\right)}. (31c)$$

E. DIVERSITY ORDER

To obtain further insights, we consider the achievable diversity order of the proposed system outage probabilities, which describes the rate at which outage probability decays as SNR grows large. Based on [9], [17], we can define the diversity order as $d_{OP_l} = -\lim_{\rho \to \infty} (\log(OP_l)/\log(\rho))$ where

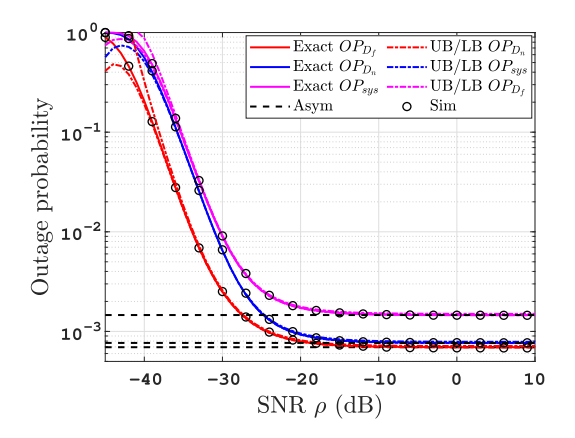


FIGURE 2. The OPs against transmitted SNR ρ with $\beta_{\ell} = 0.6$, K = 60, and $\varepsilon = 0.1$.

 $l \in \{D_f, D_n, sys\}$. It is clear from the analysis carried out in Section III-D and the result in (31), that the value of OP_I is independent of the value of ρ at high SNR, or equivalently $d_{OP_1} \propto \rho^0$, which means $d_{OP} = 0$. This result is consistent with the plots that will be shown later in Fig. 2 where the three *OPs* saturate with zero slopes.

F. BOUNDS ON OUTAGE PROBABILITY

In order to derive upper and lower bounds on the system's OPs, we utilize [39, eq. (4.20)], which gives upper and lower bounds on the Gauss hypergeometric function as in the following inequality

$$\left(1 + \frac{b}{c}z\right)^{-a} \le {}_{2}F_{1}(a, b; c; -z) \le 1 - \frac{b}{c} + \frac{b}{c}(1+z)^{-a}. \tag{32}$$

As a result, we can write the lower and upper bounds for OP_{D_f} , B_1 , and B_2 as in

$$OP_{D_{f}}^{LB} = \frac{\eta_{ff}^{k_{\delta_{ff}}} \left(1 + \frac{k_{\delta_{ff}}}{1 + k_{\delta_{ff}}} \eta_{ff}\right)^{-k_{\delta_{ff}} - k_{I_{nf}}}}{k_{\delta_{ff}} B(k_{\delta_{ff}}, k_{\chi_{nf}})}, \qquad (33a)$$

$$B_{1}^{LB} = \frac{\eta_{fn}^{k_{\delta_{fn}}} \left(1 + \frac{k_{\delta_{fn}}}{1 + k_{\delta_{fn}}} \eta_{fn}\right)^{-k_{\delta_{fn}} - k_{\chi_{nn}}}}{k_{\delta_{fn}} B(k_{\delta_{fn}}, k_{\chi_{nn}})}, \qquad (33b)$$

$$B_{1}^{LB} = \frac{\eta_{fn}^{k_{\delta_{fn}}} \left(1 + \frac{k_{\delta_{fn}}}{1 + k_{\delta_{fn}}} \eta_{fn}\right)^{-k_{\delta_{fn}} - k_{\chi_{nn}}}}{k_{\delta_{fn}} B(k_{\delta_{fn}}, k_{\chi_{nn}})}, \quad (33b)$$

$$B_{2}^{LB} = \frac{\eta_{nn}^{k_{\delta_{nn}}} \left(1 + \frac{k_{\delta_{nn}}}{1 + k_{\delta_{nn}}} \eta_{nn}\right)^{-k_{\delta_{nn}} - k_{\chi_{fn}}}}{k_{\delta_{nn}} \mathbf{B}(k_{\delta_{nn}}, k_{\chi_{fn}})}, \quad (33c)$$

$$OP_{D_f}^{UB} = \frac{\eta_{ff}^{k_{\delta ff}} \left(1 - \frac{k_{\delta ff}}{1 + k_{\delta ff}} + \frac{k_{\delta ff}}{1 + k_{\delta ff}} (1 + \eta_{ff})^{-k_{\delta ff} - k_{\chi_{nf}}}\right)}{k_{\delta_{ff}} B(k_{\delta_{ff}}, k_{\chi_{nf}})}, \quad (34a)$$

$$OP_{sys} = 1 - \left(1 - \frac{\eta_{ff}^{k_{\delta_{ff}}} {}_{2}F_{1}(k_{\delta_{ff}} + k_{\chi_{nf}}, k_{\delta_{ff}}; 1 + k_{\delta_{ff}}; -\eta_{ff})}{k_{\delta_{ff}}B(k_{\delta_{ff}}, k_{\chi_{nf}})}\right) \left(1 - \frac{\eta_{fn}^{k_{\delta_{fn}}} {}_{2}F_{1}(k_{\delta_{fn}} + k_{\chi_{nn}}, k_{\delta_{fn}}; 1 + k_{\delta_{fn}}; -\eta_{fn})}{k_{\delta_{fn}}B(k_{\delta_{fn}}, k_{\chi_{nn}})}\right) \times \left(1 - \frac{\eta_{nn}^{k_{\delta_{nn}}} {}_{2}F_{1}(k_{\delta_{nn}} + k_{\chi_{fn}}, k_{\delta_{nn}}; 1 + k_{\delta_{nn}}; -\eta_{nn})}{k_{\delta_{nn}}B(k_{\delta_{nn}}, k_{\chi_{fn}})}\right).$$
(28)

VOLUME 5. 2024 4377

$$B_{1}^{UB} = \frac{\eta_{fn}^{k_{\delta_{fn}}} \left(1 - \frac{k_{\delta_{fn}}}{1 + k_{\delta_{fn}}} + \frac{k_{\delta_{fn}}}{1 + k_{\delta_{fn}}} (1 + \eta_{fn})^{-k_{\delta_{fn}} - k_{\chi_{nn}}}\right)}{k_{\delta_{fn}} B(k_{\delta_{fn}}, k_{\chi_{nn}})}, \quad (34b)$$

$$B_2^{UB} = \frac{\eta_{nn}^{k_{\delta_{nn}}} \left(1 - \frac{k_{\delta_{nn}}}{1 + k_{\delta_{nn}}} + \frac{k_{\delta_{nn}}}{1 + k_{\delta_{nn}}} (1 + \eta_{nn})^{-k_{\delta_{nn}} - k_{\chi_{fn}}} \right)}{k_{\delta_{nn}} B(k_{\delta_{nn}}, k_{\chi_{fn}})}, \quad (34c)$$

respectively.

IV. POWER ALLOCATION OPTIMIZATION

Enhancing system performance with respect to outages represents a crucial and intricate challenge of practical significance. In pursuit of this objective, we address the optimization of power allocation to minimize the system outage probability. The proposed formulation of this minimization problem is as follows

$$\min_{\beta_f} OP_{sys}$$
 (35a)
s.t. $0.5 < \beta_f < 1$ (35b)

s.t.
$$0.5 < \beta_f < 1$$
 (35b)

$$\beta_f + \beta_n = 1. \tag{35c}$$

where OP_{svs} is given in (28). Obviously, the problem can not be solved directly since the expression of OP_{sys} is complicated. For the sake of simplicity, we use its asymptotic representation derived in Section III-D. Additionally, we introduce two further assumptions. First, we consider uniform fading across all channels, such that all Nakagami-m channels share the same severity factor denoted as m. This assumption results in the equality of $k_{\delta_{f\!f}}=k_{\delta_{n\!f}}=k_{\delta_{f\!n}}=$ $k_{\delta_{nn}} = k_{\delta}$ and $\theta_{\delta_{ff}} = \theta_{\delta_{nf}} = \theta_{\delta_{fn}} = \theta_{\delta_{nn}} = \theta_{\delta}$. Consequently,

$$\eta_{ff}^{\infty} = \eta_{fn}^{\infty} = \frac{(1 - \beta_f)\gamma_{th}^f}{\beta_f}, \quad \eta_{nn}^{\infty} = \frac{\varepsilon \beta_f \gamma_{th}^n}{(1 - \beta_f)}.$$
(36)

Furthermore, in accordance with [40], [41], [42], the values of γ_{th}^f and γ_{th}^n for BRs are consistently small, always remaining less than or equal to 0.1. Under this assumption, the value of η_{ii}^{∞} is relatively small, thus we can approximate $_2F_1(a,b;c;-\eta_{ii}^{\infty}) \approx 1$. Finally we can write the approximated OP_{sys} as

$$OP_{sys} = 1 - \left(1 - A\left(\frac{1 - \beta_f}{\beta_f}\right)^{k_\delta}\right)^2 \left(1 - B\left(\frac{\beta_f}{1 - \beta_f}\right)^{k_\delta}\right),\tag{37}$$

where $A = (\gamma_{th}^f)^{k_\delta}/k_\delta B(k_\delta, k_\delta)$ and $B = (\varepsilon \gamma_{th}^n)^{k_\delta}/k_\delta B(k_\delta, k_\delta)$. The suitability of this approximation will be graphically confirmed later in the sequel.

Lemma 1: Problem (35) has the optimal power allocation factor value as

$$\beta_f^* = \frac{1}{1 + \left(\frac{AB + \sqrt{AB(8 + AB)}}{4A}\right)^{1/k_{\delta}}},\tag{38}$$

Proof: See the Appendix.

TABLE 3. Parameter values used for simulations

Parameter	ρ (dB)	K	β_f	β_n	ε	γ_{th}^f	γ_{th}^n
Value	-40:10	60	0.6	0.4	0.1	0.1	0.1

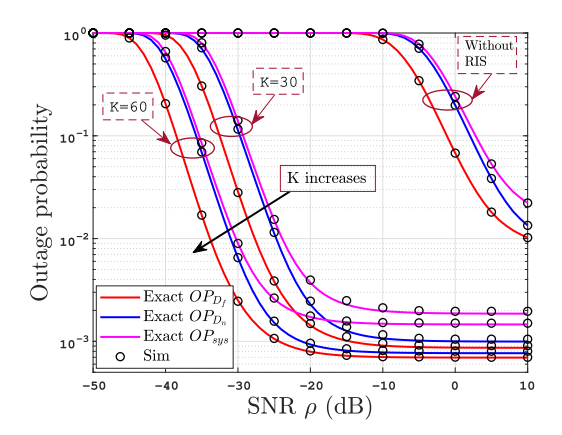


FIGURE 3. The OPs against transmitted SNR ρ with different values of K, $\beta_f = 0.6$, and $\epsilon = 0.1$.

V. RESULTS AND DISCUSSIONS

In this section, we will examine the outage performance of the proposed system. This exploration involves a comprehensive study of the effect of various system parameters, which significantly impact the system's efficiency. To substantiate our analytical findings, we conduct extensive Monte-Carlo simulations, thus providing validation for the theoretical outcomes obtained through our analytical approach. Unless mentioned otherwise, the values of parameters used in the plots are given in Table 3, also we set $m_{T_n} = m_{h_{nn}} =$ $m_{h_{fn}} = m_{L_{k,n}} = m_{g_{k,n}} = 3$, and $m_{T_f} = m_{h_{ff}} = m_{h_{nf}} =$

Figure 2 presents the OPs of the proposed system. We can clearly see the enhancement of the OPs as ρ increases, while at high SNR, it saturates due to the saturation of SINRs in (4), (5), and (6). Also, we notice the perfect agreement between the analytical and simulation results over the entire range of SNR, which proves the validity of the derived PDFs that characterize the statistical distribution of the received SINR at the BRs. Also, the figure confirms the validity of the obtained closed-form expressions for the OPs. This is in addition to the perfect agreement between the analytical and the asymptotic results at high SNR, which validates the obtained asymptotic formulas. According to Section III-E, we expect a diversity order of 0, which agrees with the results in Fig. 2 as well. Finally, the figure presents the lower and upper bounds from (33) and (34), respectively, clearly indicating their tightness.

The effect of the number of RIS reflecting elements on the outage performance is then demonstrated in Fig. 3. As expected, irrespective of whether K is high or low, the OPs decrease with the increase of ρ . The notable observation is that the increase in K significantly improves the OPs. This trend can be explained by observing that increasing K contributes to an improvement in the received

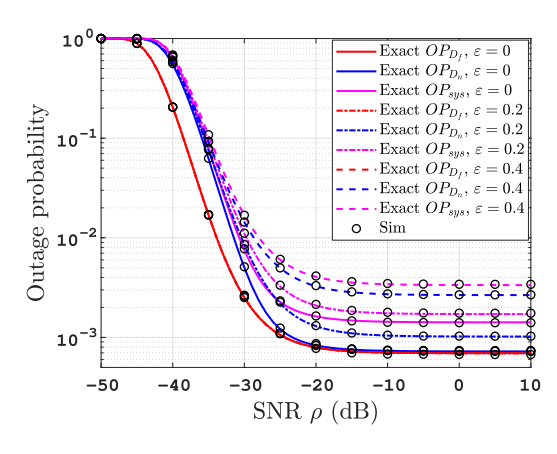


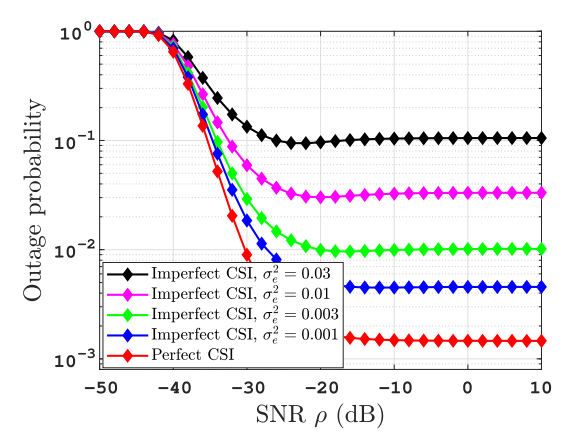
FIGURE 4. The OPs against transmitted SNR ρ with different values of ε , $\beta_I=0.6$, and K=60.

SINRs. The figure also presents a comparison between our proposed RIS-enhanced system and the conventional AmBC-NOMA benchmark without RIS. This comparison illustrates the significant performance enhancement achieved by incorporating RIS into the proposed system, which strengthens the backscattered signal.

Figure 4 illustrates the effect of the imperfect SIC, where signal detection complexity at D_n will increase. The figure shows how the value of the imperfect SIC residual ε affects the OPs curves. We assume three levels of $\varepsilon = 0, 0.2, 0.4$. From the figure, we can notice that the higher the value of ε , the worse the OPs performance. The best performance is achieved with the perfect SIC scenario ($\varepsilon = 0$), where in this case the SINR for decoding s_n suffers minimal interference level.

Fig. 5 illustrates the effect of imperfect CSI on the system outage performance. The figure is generated via simulation of the OP_{sys} with different levels of uncertainties in estimating the CSI. The uncertainty level, i.e., the error variance in CSI, σ_e^2 , is adjusted to different values such that $\sigma_e^2 \in$ {0.001, 0.003, 0.01, 0.03}. Fig. 5(a) shows that in the perfect CSI scenario, the system achieved the best performance of the OP_{sys} . As the uncertainty level increases, the system suffers a degradation in the outage performance. This degradation aligns with the fact that a higher level of uncertainty corresponds to lower-quality CSI estimation, which in turn results in a higher outage probability. Moreover, to overcome this degradation, we show in Fig. 5(b) that increasing the number of RIS elements can effectively mitigate the negative impact of the imperfect CSI. Specifically, to achieve an OP_{sys} of 10⁻¹, perfect CSI requires around 57 RIS elements while in the case of imperfect CSI with $\sigma_e = 0.001$ and with $\sigma_e = 0.01$, a RIS with 63 and 80 elements, respectively, will be needed. Additionally, increasing σ_e will degrades the system performance too, e.g., for K = 20, the OP_{sys} with $\sigma_e = 0.001$ is approximately half of the OP_{sys} with $\sigma_e = 0.01$, i.e., 0.1 vs. 0.19.

Next, Fig. 6 depicts the impact of the power allocation parameter β_f ; which varies from 0.5 to 0.99; on the OP



(a) The OP_{sys} against ρ .

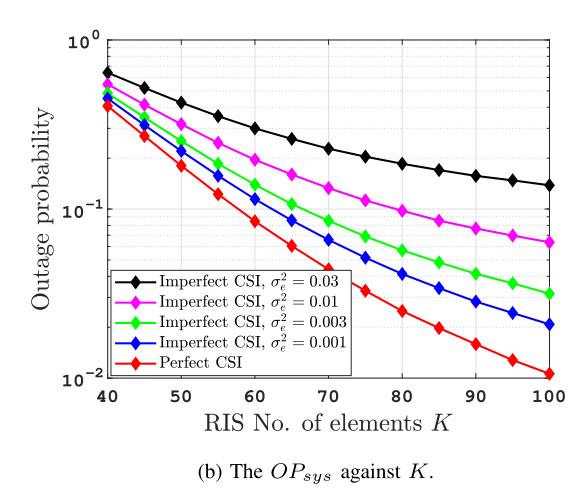


FIGURE 5. The system outage performance under different imperfect CSI scenarios.

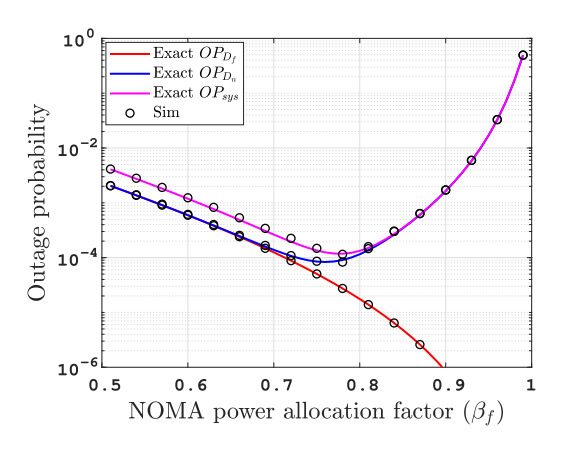


FIGURE 6. The OPs against power allocation factor β_f with $\rho = 10$ dB and K = 60.

performance with $\rho=10$ dB, K=60 and $\varepsilon=0.1$. We can see that the OP for D_f exhibits improvement with increasing β_f due to the increase in its own message power. Conversely, the OP of D_n initially experiences improvement as β_f increases since D_n must decode s_f firstly before its own message s_n . However, with the progressive rise in β_f , an inflection point is reached, since increasing β_f corresponds

VOLUME 5, 2024 4379

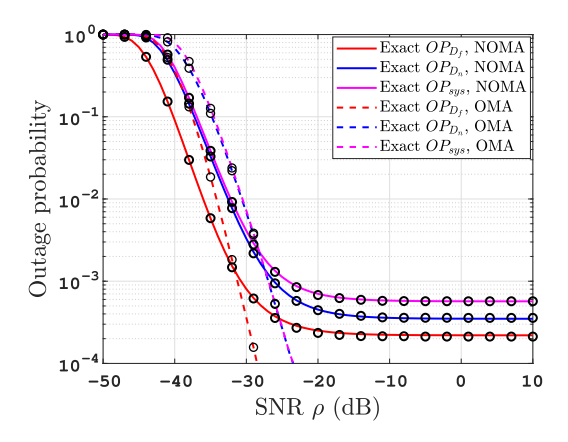


FIGURE 7. The OPs of the proposed system under different schemes NOMA and OMA for $\beta_I = 0.6$, K = 60, and $\varepsilon = 0.1$.

to a reduction in the allocated power for D_n message $(\beta_n = 1 - \beta_f)$. This consequently leads to a deterioration in the OP of D_n . Moreover, OP_{sys} mirrors the behavior of the OP of D_n , exhibiting a marginal increase in the OP value. Also, the figure shows the convexity of OP_{sys} as a function of βf , which hints at the ability to find a global optimal point β_f^* .

To assess the efficacy of the system proposed in this study, we compared its performance against a benchmark scheme; an OMA-based RIS-enhanced AmBC system. This is presented in Fig. 7, illustrating the performance contrast between the proposed NOMA-based and the OMA-based systems in terms of OPs under identical system settings. The depicted results indicate that the proposed system outperforms the benchmark in terms of OP_{D_t} , OP_{D_u} , and $OP_{D_{\text{sys}}}$ at low SNR, which is typical for low-power IoT and backscatter applications. This performance advantage can be attributed to the spectrum efficiency of the NOMAbased system, where NOMA allows for more efficient use of the available spectrum by serving multiple users simultaneously in the same resource block. This enables users with poor channel conditions to still receive signals at lower power levels by adjusting the power allocation factor, which results in reducing the likelihood of outage compared to OMA. On the other hand, at high SNR, where the received signals are strong, interference can have a more significant impact on NOMA-based systems. OMA avoids this interference by allocating separate resources to each user. From a mathematical perspective, we studied the system under the imperfect SIC scenario, which adds a residual term of interference in each of the SINR values as indicated in (4), (5) and (6). With a simple examination of these equations, we can notice that at high SNR, i.e., as $\rho \to \infty$, all three values of SINR will saturate, which leads to a lack of improvement in the outage probability terms. On the other hand, OMA avoids this scenario as the equations regarding the SINR of the OMA-based indicate a direct proportionality with the value of ρ , which suggests a continuous improvement with the increase of ρ .

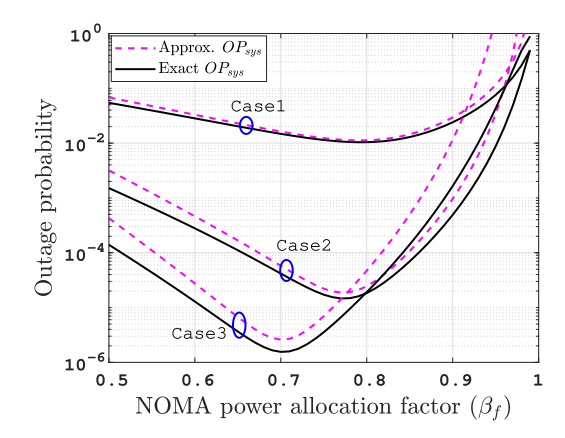


FIGURE 8. The system outage probability, exact and approximate, against power allocation factor β_ℓ with $\rho=10$ dB.

TABLE 4. Exact and approximate power allocation optimal values

β_f^*	Case 1	Case 2	Case 3	
Exact value	0.7940	0.7736	0.7030	
Approx. value	0.7917	0.7728	0.7018	

Finally, Fig. 8 depicts OP_{sys} versus the power allocation factor for different cases, namely, case 1 (m = 2, K = $50, \varepsilon = 0.1$), case 2 ($m = 5, K = 50, \varepsilon = 0.1$), and case 3 ($m = 7, K = 60, \varepsilon = 0.2$). The figure illustrates the robustness of the approximate analysis outlined in (37) in comparison to the exact formula outlined in (28), thereby confirming its suitability for optimizing the power allocation factor. Table 4 lists the exact value of β_f^* , which is obtained via plotting OP_{sys} using (28) and identifying the optimal value from the figure that minimizes system outage, while the approximate values of β_f^* are calculated using (38). It is clearly seen that the exact and approximate values are virtually indistinguishable from each other. Furthermore, the figure examines the influence of varying the fading parameter m on OP_{sys} . It is noteworthy that OP_{sys} experiences improvement with an increase in the fading parameters.

VI. CONCLUSION

In conclusion, this paper has proposed and analyzed a novel RIS-enhanced NOMA-AmBC system in the context of V2I communication. By considering Nakagami-m fading for all channels, we investigated the system's performance, particularly focusing on OPs under the realistic assumption of imperfect SIC. We derived closed-form expressions for the OPs and provided asymptotic, upper- and lower-bound expressions. Next, we formulated and solved a power allocation optimization problem to minimize the system OP. The validity of the derived analytical expressions is confirmed through Monte-Carlo simulations. Besides, we discussed the influence of different parameters on the OPs. The results indicate the suitability of the proposed system for communicating the battery-free BDs through low ambient power. Also, the study revealed significant performance improvements in the proposed RIS-enhanced NOMA-AmBC

system compared to both traditional benchmark AmBC-NOMA systems and RIS-assisted AmBC-OMA systems. This underscores the potential of the proposed system for enhancing V2I communication, offering valuable insights for the practical implementation of advanced communication systems B5G. A promising future research direction is to extend the number of BDs as well as BRs served by the system while applying a non-ideal phase shifts at the RIS.

APPENDIX PROOF OF LEMMA 1

To attain the optimal power allocation factor that minimizes the value of OP_{sys} in (37), we proceed by making the substitution $x = (1 - \beta_f)/\beta_f$, which enables us to reformulate the equation as

$$OP_{sys} = 1 - (1 - Ax^{k_{\delta}})^{2} (1 - Bx^{-k_{\delta}}).$$
 (A.1)

The optimal value of x is obtained by equating $\partial OP_{sys}/\partial x|_{x=x^*}$ to zero, where x^* is the optimal value of x. Executing this leads to

$$2Ak_{\delta}(x^{*})^{k_{\delta}-1} \left(1 - A(x^{*})^{k_{\delta}}\right) \left(1 - B(x^{*})^{-k_{\delta}}\right)$$
$$-Bk_{\delta}x^{-k_{\delta}-1} \left(1 - A(x^{*})^{k_{\delta}}\right)^{2} = 0, \tag{A.2}$$

which, after some mathematical manipulations and applying the general law of solving the quadratic equations, leads to the optimal value of x as

$$x^* = \left(\frac{AB + \sqrt{AB(8 + AB)}}{4A}\right)^{1/k_\delta}.$$
 (A.3)

Finally, a feasible optimal power allocation factor can be obtained by substituting in $\beta_f^* = 1/(1+x^*)$, which gives the optimal power allocation factor as

$$\beta_f^* = \frac{1}{1 + \left(\frac{AB + \sqrt{AB(8 + AB)}}{4A}\right)^{1/k_{\delta}}},\tag{A.4}$$

which concludes the proof.

REFERENCES

- [1] S. Raza, S. Wang, M. Ahmed, M. R. Anwar, M. A. Mirza, and W. U. Khan, "Task offloading and resource allocation for IoV using 5G NR-V2X communication," *IEEE Internet Things J.*, vol. 9, no. 13, pp. 10397–10410, Jul. 2022.
- [2] Z. Ali, W. U. Khan, A. Ihsan, O. Waqar, G. A. S. Sidhu, and N. Kumar, "Optimizing resource allocation for 6G NOMA-enabled cooperative vehicular networks," *IEEE Open J. Intell. Transp. Syst.*, vol. 2, pp. 269–281, 2021.
- [3] S. Gyawali, S. Xu, Y. Qian, and R. Q. Hu, "Challenges and solutions for cellular based V2X communications," *IEEE Commun. Surveys Tuts.*, vol. 23, no. 1, pp. 222–255, 1st Quart., 2021.
- [4] M. Zhou, Y. Li, Y. Sun, and Z. Ding, "Outage performance of RIS-assisted V2I communications with inter-cell interference," *IEEE Wireless Commun. Lett.*, vol. 12, no. 6, pp. 962–966, Jun. 2023.
- [5] B. M. ElHalawany, A. Samir, M. Elsayed, W. U. Khan, K. Wu, and E. M. Mohamed, "Outage and capacity analysis of NOMA systems over dual-hop mixed powerline-wireless channels," *ICT Exp.*, vol. 9, no. 4, pp. 601–607, 2023.
- [6] A. Samir, M. Elsayed, A. A. A. El-Banna, I. S. Ansari, K. Rabie, and B. M. ElHalawany, "Performance analysis of dual-hop hybrid RF-UOWC NOMA systems," Sensors, vol. 22, no. 12, p. 4521, 2022.

- [7] A. Samir, M. Elsayed, A. A. El-Banna, T. Y. Elganimi, K. Rabie, and B. M. ElHalawany, "Outage performance of 6G NOMA dual-hop hybrid RF-PLC system with imperfect SIC," in *Proc. 13th Int. Symp. Commun. Syst., Netw. Digit. Signal Process. (CSNDSP)*, 2022, pp. 373–378.
- [8] A. A. Salem, A. S. Ibrahim, and M. H. Ismail, "An optimization framework for RIS-based energy-efficient multi-cell NOMA systems," *Veh. Commun.*, vol. 43, Oct. 2023, Art. no. 100657.
- [9] C. Gamal et al., "Reliability of spectrum-efficient mixed satelliteunderwater systems," *IEEE Open J. Commun. Soc.*, vol. 3, pp. 2237–2244, 2022.
- [10] W. U. Khan, M. A. Jamshed, E. Lagunas, S. Chatzinotas, X. Li, and B. Ottersten, "Energy efficiency optimization for backscatter enhanced NOMA cooperative V2X communications under imperfect CSI," *IEEE Trans. Intell. Transp. Syst.*, vol. 24, no. 11, pp. 12961–12972, Nov. 2023.
- [11] A. Rastogi, S. Yadav, R. Gour, and D. S. Gurjar, "Performance analysis of ambient backscatter communication empowered IoV networks," *Phys. Commun.*, vol. 60, Oct. 2023, Art. no. 102162.
- [12] M. Elsayed, A. Samir, A. A. A. El-Banna, K. Rabie, X. Li, and B. M. ElHalawany, "Symbiotic ambient backscatter IoT transmission over NOMA-enabled network," in *Proc. IEEE Int. Conf. Commun.* (ICC), 2022, pp. 2266–2271.
- [13] H. Peng et al., "Ambient backscatter communication symbiotic intelligent transportation systems: Covertness performance analysis and optimization," *IEEE Trans. Consum. Electron.*, vol. 70, no. 1, pp. 1833–1844, Feb. 2024.
- [14] X. Li et al., "Cognitive AmBC-NOMA IoV-MTS networks with IQI: Reliability and security analysis," *IEEE Trans. Intell. Transp. Syst.*, vol. 24, no. 2, pp. 2596–2607, Feb. 2023.
- [15] X. Li, H. Liu, G. Li, Y. Liu, M. Zeng, and Z. Ding, "Effective capacity analysis of AmBC-NOMA communication systems," *IEEE Trans. Veh. Technol.*, vol. 71, no. 10, pp. 11257–11261, Oct. 2022.
- [16] N. Van Huynh, D. T. Hoang, X. Lu, D. Niyato, P. Wang, and D. I. Kim, "Ambient backscatter communications: A contemporary survey," *IEEE Commun. Surveys Tuts.*, vol. 20, no. 4, pp. 2889–2922, 4th Quart., 2018.
- [17] M. Elsayed, A. Samir, A. A. El-Banna, W. U. Khan, S. Chatzinotas, and B. M. ElHalawany, "Mixed RIS-relay NOMA-based RF-UOWC systems," in *Proc. IEEE 95th Veh. Technol. Conf. (VTC)*, 2022, pp. 1–6.
- [18] Y. Ai, F. A. P. deFigueiredo, L. Kong, M. Cheffena, S. Chatzinotas, and B. Ottersten, "Secure vehicular communications through reconfigurable intelligent surfaces," *IEEE Trans. Veh. Technol.*, vol. 70, no. 7, pp. 7272–7276, Jul. 2021.
- [19] W. Zhao, G. Wang, S. Atapattu, T. A. Tsiftsis, and X. Ma, "Performance analysis of large intelligent surface aided backscatter communication systems," *IEEE Wireless Commun. Lett.*, vol. 9, no. 7, pp. 962–966, Jul. 2020.
- [20] K.-T. Nguyen, T.-H. Vu, and S. Kim, "A unified framework analysis for reconfigurable intelligent surface-aided coordinated NOMA systems," *IEEE Trans. Veh. Technol.*, vol. 72, no. 11, pp. 15115–15120, Nov. 2023.
- [21] F. R. Ghadi, M. Kaveh, and D. Martín, "Performance analysis of RIS/STAR-IOS-aided V2V NOMA/OMA communications over composite fading channels," *IEEE Trans. Intell. Veh.*, vol. 9, no. 1, pp. 279–286, Jan. 2024.
- [22] U. S. Toro, M. Elsayed, B. M. ElHalawany, and K. Wu, "Performance analysis of intelligent reflecting surfaces in ambient backscattering NOMA systems," *IEEE Trans. Veh. Technol.*, vol. 73, no. 2, pp. 2854– 2859. Feb. 2024.
- [23] J. Zuo, Y. Liu, L. Yang, L. Song, and Y.-C. Liang, "Reconfigurable intelligent surface enhanced NOMA assisted backscatter communication system," *IEEE Trans. Veh. Technol.*, vol. 70, no. 7, pp. 7261–7266, Jul. 2021.
- [24] J. Hu, Y.-C. Liang, and Y. Pei, "Reconfigurable intelligent surface enhanced multi-user MISO symbiotic radio system," *IEEE Trans. Commun.*, vol. 69, no. 4, pp. 2359–2371, Apr. 2021.
- [25] M. Elhattab, M. A. Arfaoui, C. Assi, and A. Ghrayeb, "RIS-assisted joint transmission in a two-cell downlink NOMA cellular system," *IEEE J. Sel. Areas Commun.*, vol. 40, no. 4, pp. 1270–1286, Apr. 2022.

4381

- [26] S. Ma, G. Wang, R. Fan, and C. Tellambura, "Blind channel estimation for ambient backscatter communication systems," *IEEE Commun. Lett.*, vol. 22, no. 6, pp. 1296–1299, Jun. 2018.
- [27] F. Rezaei, D. Galappaththige, C. Tellambura, and A. Maaref, "Time-spread pilot-based channel estimation for backscatter networks," *IEEE Trans. Commun.*, vol. 72, no. 1, pp. 434–449, Jan. 2024.
- [28] Z. Xie, W. Yi, X. Wu, Y. Liu, and A. Nallanathan, "Downlink multi-RIS aided transmission in backhaul limited networks," *IEEE Wireless Commun. Lett.*, vol. 11, no. 7, pp. 1458–1462, Jul. 2022.
- [29] X. Gu et al., "On the performance of cooperative NOMA downlink: A RIS-aided D2D perspective," *IEEE Trans. Cogn. Commun. Netw.*, vol. 9, no. 6, pp. 1610–1624, Dec. 2023.
- [30] A.-A. A. Boulogeorgos and A. Alexiou, "Performance analysis of reconfigurable intelligent surface-assisted wireless systems and comparison with relaying," *IEEE Access*, vol. 8, pp. 94463–94483, 2020.
- [31] S. Bisen, P. Shaik, and V. Bhatia, "On performance of energy harvested cooperative NOMA under imperfect CSI and imperfect SIC," *IEEE Trans. Veh. Technol.*, vol. 70, no. 9, pp. 8993–9005, Sep. 2021.
- [32] V. Aswathi and A. V. Babu, "Full/half duplex cooperative NOMA under imperfect successive interference cancellation and channel state estimation errors," *IEEE Access*, vol. 7, pp. 179961–179984, 2019
- [33] V.-D. Phan et al., "Performance of cooperative communication system with multiple reconfigurable intelligent surfaces over Nakagami-*m* fading channels," *IEEE Access*, vol. 10, pp. 9806–9816, 2022.

- [34] T. Wang, G. Chen, and J. P. Coon, "Performance analysis of RIS-assisted full-duplex communication over correlated Nakagamim fading channel," *IEEE Trans. Veh. Technol.*, vol. 73, no. 3, pp. 3430–3444, Mar. 2024.
- [35] S. Kim, J. Y. Lee, and D. K. Sung, "A shifted gamma distribution model for long-range dependent internet traffic," *IEEE Commun. Lett.*, vol. 7, no. 3, pp. 124–126, Mar. 2003.
- [36] N. B. Norman L. Johnson, and S. Kotz, Continuous Univariate Distributions, 2nd ed. New York, NY, USA: Wiley, 1994.
- [37] Y. Ni, Y. Liu, Q. Wang, Y. Wang, H. Zhao, and H. Zhu, "Vehicular networks under Nakagami-m fading channels: Outage probability and ergodic achievable rate," *IEEE Access*, vol. 8, pp. 121501–121512, 2020.
- [38] I. Gradshteyn and I. Ryzhik, Table of Integrals, Series, and Products, 7th ed. Amsterdam, The Netherlands: Elsevier, 2014.
- [39] Y. L. Luke, "Inequalities for generalized hypergeometric functions," J. Approx. Theory, vol. 5, no. 1, pp. 41–65, 1972.
- [40] Q. Zhang, L. Zhang, Y.-C. Liang, and P.-Y. Kam, "Backscatter-NOMA: A symbiotic system of cellular and Internet-of-Things networks," *IEEE Access*, vol. 7, pp. 20000–20013, 2019.
- networks," *IEEE Access*, vol. 7, pp. 20000–20013, 2019.

 [41] S. Solanki, S. Gautam, S. K. Sharma, and S. Chatzinotas, "Ambient backscatter assisted co-existence in aerial-IRS wireless networks," *IEEE Open J. Commun. Soc.*, vol. 3, pp. 608–621, 2022.
- [42] X. Li, M. Zhao, Y. Liu, L. Li, Z. Ding, and A. Nall, "Secrecy analysis of ambient backscatter NOMA systems under I/Q imbalance," *IEEE Trans. Veh. Technol.*, vol. 69, no. 10, pp. 12286–12290, Oct. 2020.